



Danish and British dementia *ITM2b/BRI2* mutations reduce BRI2 protein stability and impair glutamatergic synaptic transmission

Received for publication, August 17, 2020, and in revised form, November 9, 2020. Published, Papers in Press, November 10, 2020.

<https://doi.org/10.1074/jbc.RA120.015679>

Tao Yin¹ , Wen Yao¹, Alexander D. Lemenze² , and Luciano D'Adamo^{1,*}

From the ¹Department of Pharmacology, Physiology & Neuroscience New Jersey Medical School, Brain Health Institute, Jacqueline Krieger Klein Center in Alzheimer's Disease and Neurodegeneration Research, Rutgers, The State University of New Jersey, Newark, New Jersey, USA; ²Department of Pathology, Immunology, and Laboratory Medicine, New Jersey Medical School, The State University of New Jersey, Newark, New Jersey, USA

Edited by Paul Fraser

Mutations in *integral membrane protein 2B (ITM2b/BRI2)* gene cause familial British and Danish dementia (FBD and FDD), autosomal dominant disorders characterized by progressive cognitive deterioration. Two pathogenic mechanisms, which may not be mutually exclusive, have been proposed for FDD and FBD: 1) loss of BRI2 function; 2) accumulation of amyloidogenic mutant BRI2-derived peptides, but the mechanistic details remain unclear. We have previously reported a physiological role of BRI2 in excitatory synaptic transmission at both presynaptic termini and postsynaptic termini. To test whether pathogenic *ITM2b* mutations affect these physiological BRI2 functions, we analyzed glutamatergic transmission in FDD and FBD knock-in mice, which carry pathogenic FDD and FBD mutations into the mouse endogenous *Itm2b* gene. We show that in both mutant lines, spontaneous glutamate release and AMPAR-mediated responses are decreased, while short-term synaptic facilitation is increased, effects similar to those observed in *Itm2b*^{KO} mice. *In vivo* and *in vitro* studies show that both pathogenic mutations alter maturation of BRI2 resulting in reduced levels of functional mature BRI2 protein at synapses. Collectively, the data show that FDD and FBD mutations cause a reduction of BRI2 levels and function at synapses, which results in reduced glutamatergic transmission. Notably, other genes mutated in Familial dementia, such as *APP*, *PSEN1/PSEN2*, are implicated in glutamatergic synaptic transmission, a function that is altered by pathogenic mutations. Thus, defects in excitatory neurotransmitter release may represent a general and convergent mechanism leading to neurodegeneration. Targeting these dysfunction may offer a unique disease modifying method of therapeutic intervention in neurodegenerative disorders.

ITM2b/BRI2 gene is a gene that codes a type II membrane protein called BRI2. The immature BRI2 precursor (imBRI2) is cleaved at the C-terminus by proprotein convertase to produce the mature NH₂-terminal BRI2 (mBRI2) and a COOH-terminal peptide of 23 amino acid called Bri23 (1). Two

autosomal dominant mutations in *ITM2b/BRI2* cause FDD and FBD. The FDD mutation consists of a 10-nucleotide duplication one codon before the normal stop codon (2). This produces a frameshift in the BRI2 sequence generating a precursor protein 11 amino acids larger than normal. In the British kindred, a point mutation at the stop codon of *BRI2* results in a read-through of the 3'-untranslated region and the synthesis of a BRI2 molecule containing 11 extra amino acids at the COOH-terminus (3). Convertase-mediated cleavage of immature mutant Danish and British BRI2 generates two distinct 34 amino acid long peptides, called ADan and ABri, respectively. Both peptides are deposited as amyloid fibrils. For clarity, we will refer to the wild-type imBRI2 as BRI2-Bri23, to the Danish mutant imBRI2 as BRI2-ADan, and to the British mutant imBRI2 as BRI2-ABri. Since all three imBRI2 proteins form the same mBRI2 polypeptide, all mBRI2 proteins will be referred to as mBRI2.

Using a genetic approach to inactivate *Itm2b* in either presynaptic (CA3), or postsynaptic (CA1), or both (CA3+CA1) neurons of the hippocampal Schaeffer-collateral pathway (SC-CA3>CA1 synapses) in mice, we found a physiological role of Bri2 in the excitatory synaptic transmission (4). Loss of Bri2 impairs glutamatergic neurotransmitter release and AMPAR-mediated responses in SC-CA3>CA1 synapses by a presynaptic and postsynaptic mechanism, respectively. This evidence suggests that Bri2 facilitates glutamate transmission *via* both presynaptic and postsynaptic mechanism. Given the relevance of excitatory synaptic transmission to cognition and that BRI2 mutations cause neurodegeneration and dementia in humans, we tested whether the pathogenic Danish and British dementia mutations will alter, one way or another, this physiological function of BRI2. To test this hypothesis, we studied glutamatergic neurotransmission in SC-CA3>CA1 synapses of mice carrying the pathogenic Danish and British dementia mutations (*Itm2b*^{D/D} and *Itm2b*^{B/B} mice) into the *Itm2b* mouse gene (5–7). We choose a knock-in (KI) approach because: a) KIs mimic familial dementia genetics and make no assumption about pathogenic mechanisms; b) expression of mutant genes is controlled by endogenous regulatory elements, thereby allowing us to test the hypothesis in a biologically relevant

* For correspondence: Luciano D'Adamo, luciano.dadamio@rutgers.edu.

Itm2b and excitatory transmission

model organism. This strategy allows examination of the effects of pathogenic *Itm2b* mutations on the function of Bri2 in excitatory synaptic transmission on both presynaptic and postsynaptic neurons of the Schaeffer-collateral pathway.

Results

Pathogenic Bri2 mutations impair glutamatergic transmission at excitatory hippocampal SC-CA3>CA1 synapses

Itm2b^{D/D} and *Itm2b*^{B/B} mice were derived as described previously (5–7). To test whether these pathogenic mutations alter the synaptic function of Bri2 in the excitatory synaptic transmission at SC-CA3>CA1 synapses (4), we compared the following genotypes: *Itm2b*^{WT/WT}, *Itm2b*^{KO/KO} (mice carrying two knockout *Itm2b* alleles), *Itm2b*^{D/D} (mice carrying two *Itm2b* alleles with the Danish mutation), and *Itm2b*^{B/B} (mice carrying two *Itm2b* alleles with the British mutation). Synaptic transmission was studied in 4 to 6-month-old *Itm2b*^{WT/WT} (three males and three females), *Itm2b*^{KO/KO} (three males and three females), *Itm2b*^{D/D} (three males and three females), and *Itm2b*^{B/B} (four males and three females) mice. First, we analyzed miniature excitatory postsynaptic currents (mEPSC), the frequency of which is also determined, in part, by the probability of synaptic vesicles release (*Pr*) (8): a decrease in *Pr* leads to a decrease in frequency and vice versa. As previously shown (4) and in accord with the hypothesis that endogenous Bri2 facilitates glutamate release, the frequency of mEPSC was reduced in *Itm2b*^{KO/KO} mice (Fig. 1, A–C). The British and Danish *Itm2b* mutations acted analogously, both causing a reduction in the frequency of mEPSC (Fig. 1, A–C).

The amplitude of mEPSC is dependent on postsynaptic AMPA (α -amino-3-hydroxy-5-methyl-4-isoxazole propionic acid) receptor (AMPA-mediated responses). Consistently with our previous report, the amplitude of mEPSC was significantly decreased in *Itm2b*^{KO/KO} mice (Fig. 1, D, E and G). Like for the mEPSC frequency, *Itm2b*^{D/D} and *Itm2b*^{B/B} mice showed a phenotype similar to *Itm2b*^{KO/KO} animals (Fig. 1, D, E and G). The decay time of mEPSC was slightly higher in all mutant lines: however, this slight increase reached statistical significance only for the *Itm2b*^{D/D} mice (Fig. 1F).

Next, we measured AMPAR and NMDAR-dependent synaptic responses. Consistent with the hypothesis that Bri2 boosts AMPAR-mediated responses, the AMPA/NMDA ratio was reduced in *Itm2b*^{KO/KO} mice (Fig. 1H). Once again, a similar decrease was observed in *Itm2b*^{D/D} and *Itm2b*^{B/B} mice (Fig. 1H).

Finally, we examined the effect of *Itm2b* inactivation and pathogenic mutations on paired-pulse facilitation (PPF). PPF is a form of short-term synaptic plasticity that is determined, at least in part, by changes in *Pr* of glutamatergic synaptic vesicles (SV): inversely to mEPSC frequency, a decrease in *Pr* leads to an increase in facilitation and vice versa (8). Previous studies on older mice showed that PPF at 50 ms interstimulus interval (ISI), but not at 200 ms ISI, was significantly increased in *Itm2b*^{KO/KO} mice (4). In this set of studies, facilitation at 50 ms ISI was increased in *Itm2b*^{KO/KO}: however, this increase did not reach statistical significance (Fig. 1I). This discrepancy with our previous report is probably due to the lower number of

recordings analyzed here. Yet, both *Itm2b*^{D/D} and *Itm2b*^{B/B} mice showed increased PPF as compared with control *Itm2b*^{WT/WT} animals at 50 ms ISI (Fig. 1). Overall, our data indicate that *Itm2b* inactivation and both Danish and British pathogenic *Itm2b* mutations alter glutamatergic synaptic transmission at excitatory hippocampal SC-CA3>CA1 synapses analogously.

Reduced synaptic levels of mBri2 in *Itm2b*^{B/B} and *Itm2b*^{D/D} mice

The evidence that genetic inactivation of Bri2 expression in pre- and postsynaptic neurons reduced excitatory synaptic transmission at hippocampal SC-CA3>CA1 synapse indicates that neuronal, and perhaps synaptic, mBri2 expression is important for physiological glutamate transmission. To determine whether the synaptic impairment in *Itm2b*^{B/B} and *Itm2b*^{D/D} mice is associated with loss of mBri2 at synapses, we examined Bri2 expression in synaptoneurosome fraction (Fig. 2A shows the quality of synaptosomal fractions) prepared from whole brain lysates of 4 to 6-month-old mice (*n* = 6 for each genotype). We observed the following: 1) Bri2 is present in synaptoneurosome (Fig. 2, A–B); 2) only mBri2 is found in synaptoneurosome (Fig. 2, A–B), which is consistent with the evidence that only mature Bri2 transported to surface membrane (9); 3) mBri2 expression is significantly and similarly reduced in *Itm2b*^{B/B} and *Itm2b*^{D/D} mice compared with *Itm2b*^{WT/WT} mice (Fig. 2, B–C). These results may explain why glutamatergic synaptic transmission is similarly affected in *Itm2b*^{KO/KO}, *Itm2b*^{B/B}, and *Itm2b*^{D/D} mice.

The synaptoneurosome preparation includes synaptic elements from both excitatory and inhibitory neurons. To ascertain *Itm2b* mRNA expression in various neuronal populations, we analyzed publicly available scRNA-seq to test *Itm2b* mRNA coexpression with GABA_A-receptor (*Gabra1*, *Gabrb3*, *Gabrg2*), AMPA-receptor (*Gria1*, *Gria2*, *Gria3*, *Gria4*), and NMDA-receptor (*Grin1*, *Grin2a*, *Grin2b*) genes. This analysis shows similar levels of coexpression of *Itm2b* with these neuronal markers (Fig. 2D). In addition, we determine coexpression of *Itm2b* with *Slc32a1*, which encodes for the vesicular inhibitory amino acid transporter *Viaat* and is a marker of inhibitory neurons, *Slc17a7* and *Slc17a6*, which encode for vesicular glutamate transporter 1 *Vglut1* and vesicular glutamate transporter 2 *Vglut2*, respectively, and are markers of excitatory neurons. The results suggest that *Itm2b* mRNA is equally expressed in excitatory and inhibitory neurons (Fig. 2D). This data suggest that it will be worth, in future experiments, testing the role of Bri2 and the effects of the Danish and British mutations on GABAergic transmission as well.

Trafficking and maturation of mutant human BRI2 proteins are altered in transfected cell line

To investigate how the British and Danish pathogenic mutations affect BRI2 expression, we transfected HeLa cell with constructs driving expression of either BRI2-Bri23, BRI2-Adan, or BRI2-ABri fused to a Flag-peptide epitope at the

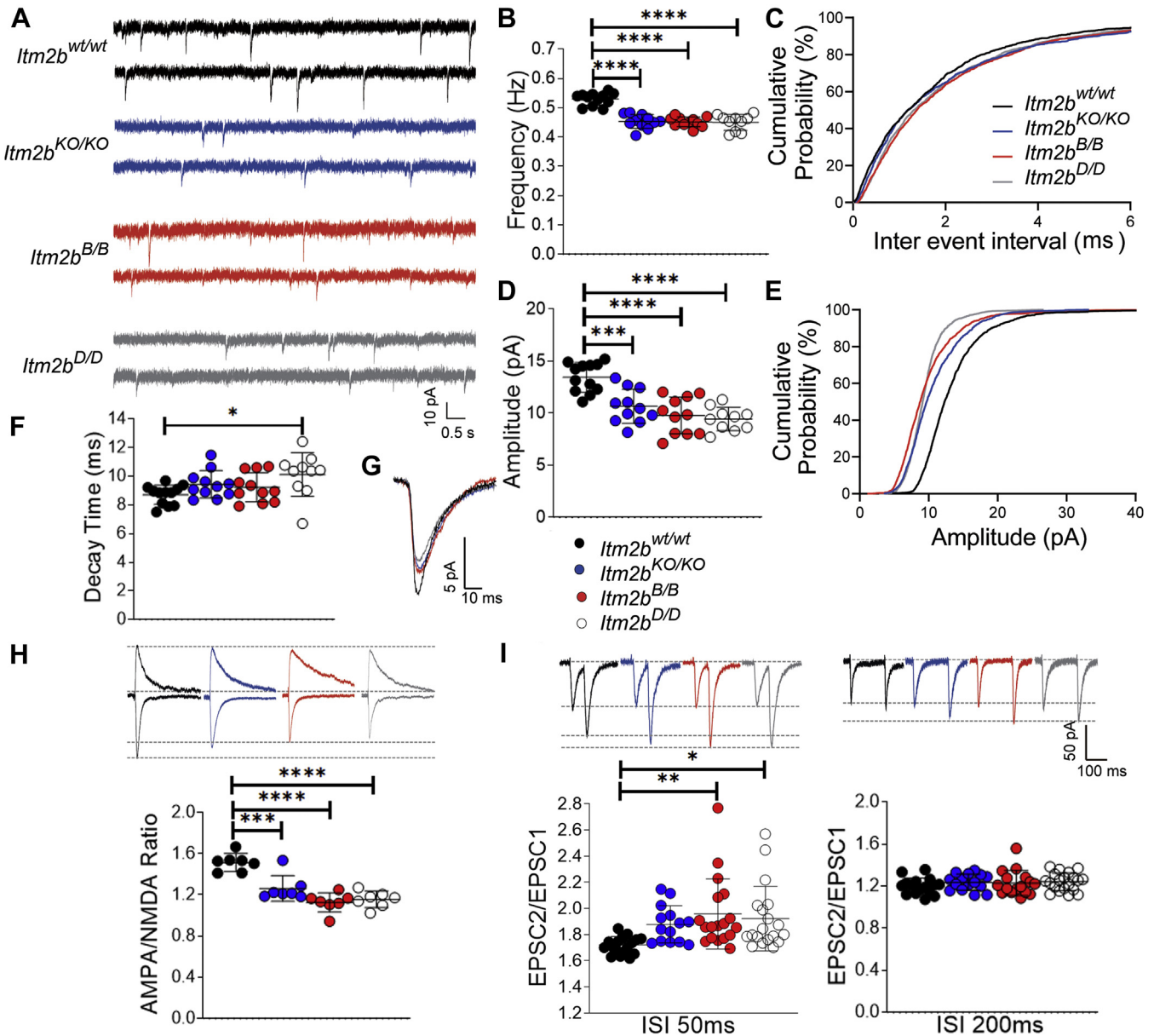


Figure 1. The Danish and British mutations reduce glutamatergic synaptic transmission at hippocampal SC-CA3>CA1 synapses. *A*, representative recording traces of mEPSC at SC-CA3>CA1 pyramidal cell synapses. *B*, the deletion of *Itm2b* (*Itm2b*^{KO/KO}), the British and Danish mutations (*Itm2b*^{B/B} and *Itm2b*^{D/D}) cause a significant decrease in mEPSC frequency [ANOVA summary, $F_{(3, 40)} = 35.44, p < 0.0001^{****}$; post-hoc Tukey's multiple comparisons test: *Itm2b*^{WT/WT} versus *Itm2b*^{KO/KO}, $p < 0.0001^{****}$; *Itm2b*^{WT/WT} versus *Itm2b*^{B/B}, $p < 0.0001^{****}$; *Itm2b*^{WT/WT} versus *Itm2b*^{D/D}, $p < 0.0001^{****}$; *Itm2b*^{-/-} versus *Itm2b*^{B/B}, $p = 0.9982$ (ns); *Itm2b*^{KO/KO} versus *Itm2b*^{D/D}, $p = 0.9825$ (ns); *Itm2b*^{B/B} versus *Itm2b*^{D/D}, $p = 0.9969$ (ns)]. *C*, cumulative probability of AMPAR-mediated mEPSC frequency inter event intervals. *D*, *Itm2b*^{KO/KO}, *Itm2b*^{B/B} and *Itm2b*^{D/D} mice show a significant decrease in mEPSC amplitude [ANOVA summary, $F_{(3, 40)} = 16.59, p < 0.0001^{****}$; post-hoc Tukey's multiple comparisons test: *Itm2b*^{WT/WT} versus *Itm2b*^{KO/KO}, $p = 0.0004^{***}$; *Itm2b*^{WT/WT} versus *Itm2b*^{B/B}, $p < 0.0001^{****}$; *Itm2b*^{WT/WT} versus *Itm2b*^{D/D}, $p < 0.0001^{****}$; *Itm2b*^{KO/KO} versus *Itm2b*^{B/B}, $p = 0.5223$ (ns); *Itm2b*^{KO/KO} versus *Itm2b*^{D/D}, $p = 0.2569$ (ns); *Itm2b*^{B/B} versus *Itm2b*^{D/D}, $p = 0.9516$ (ns)]. *E*, cumulative probability of AMPAR-mediated mEPSC amplitude. *F*, in contrast, decay time of mEPSC was modestly increased, but only in the *Itm2b*^{D/D} mice [$F_{(2, 30)} = 3.284, p = 0.0304^*$; post-hoc Tukey's multiple comparisons test: *Itm2b*^{WT/WT} versus *Itm2b*^{KO/KO}, $p = 3590$ (ns); *Itm2b*^{WT/WT} versus *Itm2b*^{B/B}, $p = 0.6339$ (ns); *Itm2b*^{WT/WT} versus *Itm2b*^{D/D}, $p = 0.0176^*$; *Itm2b*^{KO/KO} versus *Itm2b*^{B/B}, $p = 0.9585$ (ns); *Itm2b*^{KO/KO} versus *Itm2b*^{D/D}, $p = 0.4707$ (ns); *Itm2b*^{B/B} versus *Itm2b*^{D/D}, $p = 0.2433$ (ns)]. *G*, average mEPSC of the three groups depicts differences in amplitude. *H*, AMPA/NMDA ratio is significantly decreased in all three mutant mice [ANOVA summary, $F_{(3, 24)} = 22.73, p < 0.0001^{****}$; post-hoc Tukey's multiple comparisons test: *Itm2b*^{WT/WT} versus *Itm2b*^{KO/KO}, $p = 0.0004^{***}$; *Itm2b*^{WT/WT} versus *Itm2b*^{B/B}, $p < 0.0001^{****}$; *Itm2b*^{WT/WT} versus *Itm2b*^{D/D}, $p < 0.0001^{****}$; *Itm2b*^{KO/KO} versus *Itm2b*^{B/B}, $p = 0.0679$ (ns); *Itm2b*^{KO/KO} versus *Itm2b*^{D/D}, $p = 0.1988$ (ns); *Itm2b*^{B/B} versus *Itm2b*^{D/D}, $p = 0.9416$ (ns)]. Representative traces are shown on top of the graph (traces are averaged from 20 sweeps). *I*, average PPF at 50 ms (left panel) and 200 ms (right panel) Inter stimulus Interval (ISI) shows that PPF is increased in *Itm2b*^{B/B} and *Itm2b*^{D/D} mice, but only at 50 ms ISI [PPF at 50 ms ISI: ANOVA summary, $F_{(3, 65)} = 4.855, p = 0.0041^{**}$; post-hoc Tukey's multiple comparisons test: *Itm2b*^{WT/WT} versus *Itm2b*^{KO/KO}, $p = 0.1358$ (ns); *Itm2b*^{WT/WT} versus *Itm2b*^{B/B}, $p < 0.0043^{**}$; *Itm2b*^{WT/WT} versus *Itm2b*^{D/D}, $p = 0.0176^*$; *Itm2b*^{KO/KO} versus *Itm2b*^{B/B}, $p = 0.06888$ (ns); *Itm2b*^{KO/KO} versus *Itm2b*^{D/D}, $p = 0.9256$ (ns); *Itm2b*^{B/B} versus *Itm2b*^{D/D}, $p = 0.9506$ (ns)]; PPF at 200 ms ISI: ANOVA summary $F_{(3, 63)} = 0.7463, p = 0.5285$ (ns)]. Representative traces are shown on top of the panels. Data are represented as mean \pm SD and were analyzed by ordinary one-way ANOVA followed by post-hoc Tukey's multiple comparisons test when ANOVA showed significant differences. We used $n = 6$ animals for each genotype, three males and three females.

Itm2b and excitatory transmission

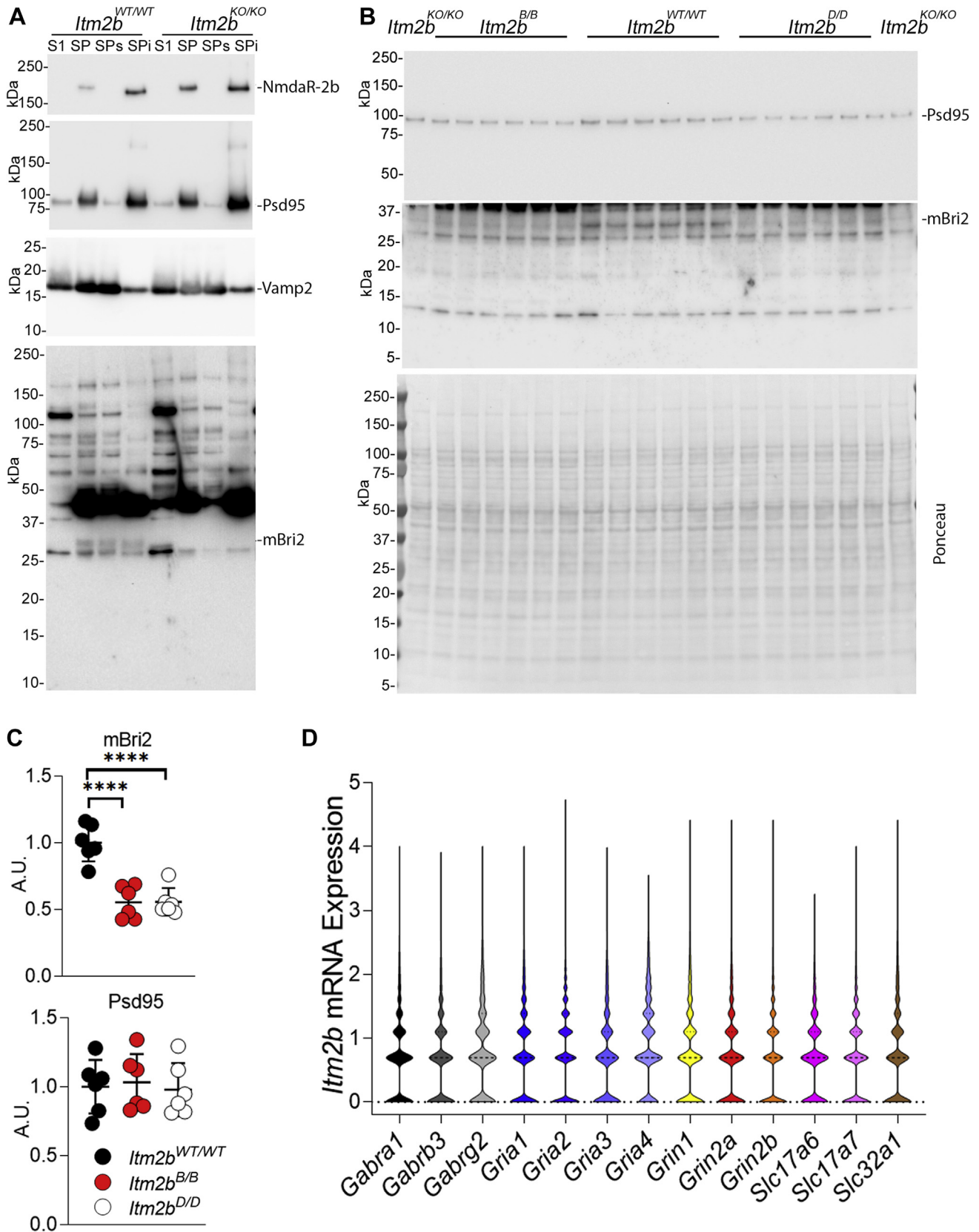


Figure 2. Expression of mBri2 is reduced in synaptoneurosome fractions derived from *Itm2b*^{B/B} and *Itm2b*^{D/D} mice. A, synaptoneurosome fractions (SP) were separated from total brain homogenates (S1) of *Itm2b*^{WT/WT} and *Itm2b*^{KO/KO} and were further separated into triton-X soluble (SPs) and insoluble fraction (SPi). Presynaptic proteins (such as Vamp2) are enriched in SP as compared with S1 and are mainly distributed in the SPs fraction. Postsynaptic proteins (such as NmdaR-2b and Psd95) are enriched in SP as compared with S1 and are mainly distributed in the SPi fraction. These data attest the good quality of the SP preparation. Consistent with pre- and postsynaptic activity of Bri2, mBri2 is found in both pre- and postsynaptic enriched fractions. Since

NH2-terminus (*ITM2b^{F-WT}*, *ITM2b^{F-D}*, and *ITM2b^{F-B}*, driving expression of F-BRI2-Bri23, F-BRI2-Adan, and F-BRI2-ABri, respectively). The levels of mF-BRI2 were significantly higher in *Itm2b^{F-WT}* lysate as compared with *Itm2b^{F-B}* and *Itm2b^{F-D}* (Fig. 3, A–B). Also, the levels of F-BRI2-Bri23 were significantly higher compared with F-BRI2-ADan and F-BRI2-ABri (Fig. 3, A–B). In addition, the ratio of mF-BRI2 to immature F-BRI2 precursor proteins was lower in *Itm2b^{F-B}* and *Itm2b^{F-D}* as compared with *Itm2b^{F-WT}* transfected cells: this difference was highly significant for *Itm2b^{F-D}* samples (Fig. 3, A–B). Although potential differences in transfection efficiencies may be confounding factors, together these data suggest that the British and Danish pathogenic mutations reduce stability and maturation of precursor BRI2-ADan and BRI2-ABri as compared with wild-type BRI2-Bri23.

To further analyze the effect of pathogenic mutation on BRI2 polypeptides trafficking to cell membranes, HeLa cells transfected with BRI2 constructs were surface biotinylated, and the lysates were precipitated with streptavidin (SA) beads to isolate cell membrane proteins (fraction B). Unbound fraction (supernatant fraction U) contains proteins that are not present on the cell membrane and/or exposed to extracellular space. Analysis of the total lysate (T) and fractions B and U confirmed that mBRI2, but not BRI2-Bri23, BRI2-Adan, and BRI2-ABri, was present on the cell surface (fraction B, Fig. 3, C–D). Given the reduction in mBRI2 levels, *Itm2b^{F-B}* and *Itm2b^{F-D}* transfected cells presented significantly reduced levels of mBRI2 localized to the plasma membrane compared with *Itm2b^{F-WT}* transfected cells (fraction B, Fig. 3, C–D).

Plasma membrane BRI2 undergoes an additional cleavage by ADAM10 in its ectodomain (10). This cleavage releases a soluble variant of BRI2 and a membrane-bound BRI2 N-terminal fragment (BRI2-NTF). As shown in Figure 3C, BRI2-NTFs are visible (and are biotinylated indicating the presence on plasma membranes) in cells transfected with WT BRI2 but not FDD and FBD mutant BRI2, supporting the notion that more mBRI2 is generated from BRI2-Bri23 as compared with BRI2-ADan and BRI2-ABri.

While in synaptoneurosomes (Fig. 2B) the two pathogenic mutations seem to reduce equally mBri2 levels, there is a more pronounced difference for BRI2-ADan than BRI2-ABri on mBRI2 in HeLa cells, suggesting that the Danish and British mutations may impair maturation of Bri2 in a quantitatively distinct manner in different cell types.

To better describe trafficking of wild-type and mutant BRI2 proteins, we transfected the F-BRI2 constructs in N2A cells with differentiation and visualized the distribution of BRI2 polypeptides by immunocytochemistry (Fig. 4A). This experiment is not used as a proxy for synaptic localization of

BRI2. We defined two types of BRI2 staining patterns: identifiable surface membrane staining (compatible with plasma membrane BRI2 localization) versus internal staining compatible with BRI2 localization in endoplasmic reticulum, Golgi apparatus, and/or other cytosolic organelles (Fig. 4B). Based on these parameters, we quantified a significant reduction of cells with identifiable surface membrane staining but a significant increase in cells with internal staining in *Itm2b^{F-B}* and *Itm2b^{F-D}* transfected cells compared with *Itm2b^{F-WT}* transfected cells (Fig. 4C). Consistent with these changes, surface biotinylation of transfected N2A cells showed reduced levels of mBRI2 localized to the plasma membrane in *Itm2b^{F-B}* and *Itm2b^{F-D}* transfected cells compared with *Itm2b^{F-WT}* transfected cells (Fig. 4C). Also, in this experiment, BRI2-NTFs are visible and detectable on the plasma membrane in cells transfected with WT BRI2 but not FDD and FBD mutant BRI2.

In summary, these observations indicate that pathogenic mutation reduces maturation and plasma membrane localization of mBRI2.

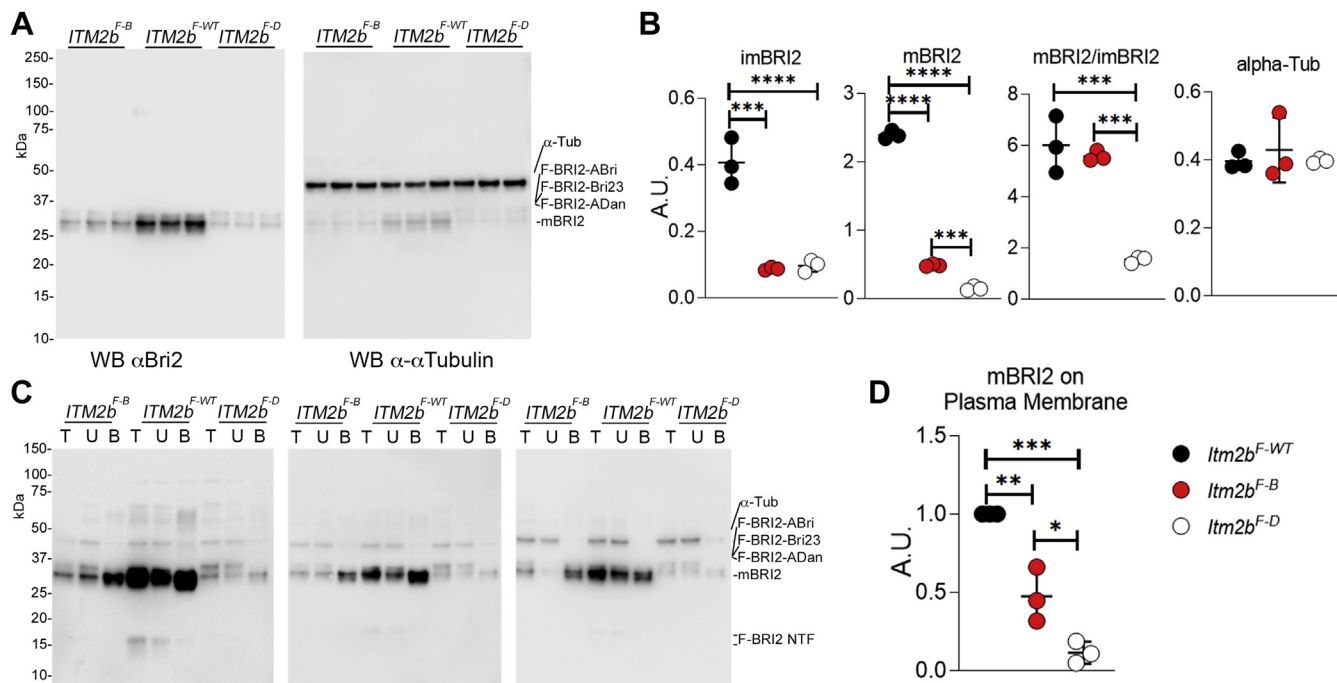
Increased lysosomal mediated degradation of BRI2-ADan and BRI2-ABri

Transmembrane proteins that enter the ER, but fail to attain the native structure, are rapidly degraded to prevent toxic accumulation of aberrant gene products. These proteins are delivered to endo-lysosome for clearance by autophagic and nonautophagic pathways collectively defined as ER-to-lysosomes-associated degradation (ERLAD) (11). To investigate whether such a mechanism could underlie the maturation deficit and the reduction of mBRI2 caused by the Danish/British mutations, we prepared primary hippocampus neurons from *Itm2b^{WT/WT}*, *Itm2b^{B/B}*, and *Itm2b^{D/D}* mice. Primary neurons were treated with the lysosomal inhibitor chloroquine.

The first noteworthy observation is that without treatment, the steady-state levels of mBri2, Bri2-NTF as well as the ratio of m/im forms of Bri2 were significantly reduced in *Itm2b^{B/B}* and *Itm2b^{D/D}* neurons as compared with *Itm2b^{WT/WT}* neurons (Fig. 5A). This observation parallels what seen in cell lines expressing human wild-type and mutant BRI2. The evidence that chloroquine significantly reduced the LC3A I/LC3A II and LC3B I/LC3B II ratios indicates inhibition of lysosome-mediated degradation. In contrast, GAPDH levels are not changed by chloroquine treatment indicating specificity and lack of toxicity (Fig. 5, A–B). In neurons derived from *Itm2b^{WT/WT}* hippocampi, chloroquine caused a significant and predominant accumulation of mBri2, suggesting that mBri2 may be degraded by lysosome after endocytosis from plasma

the anti-Bri2 antibody used in WB has many background bands, we always use *Itm2b^{KO/KO}* samples as a negative control to determine with certainty which band corresponds to Bri2. B, analysis of mBri2 and PSD95 expression in synaptoneurosomes of 4 to 6-month-old mice (we used three male and three female mice for each genotype, *Itm2b^{WT/WT}*, *Itm2b^{D/D}*, and *Itm2b^{B/B}*). The red ponceau staining, which indicates the total protein loaded on the gel, of the membrane used for Western immunoblot analysis is also shown. C, the density of mBri2 and Psd95 was measured and normalized to red ponceau intensity. D, violin plot illustrating the normalized expression values of *Itm2b* across selected gene positive cells. Cells were respective gene positive with a normalized expression value greater than 1. Data are represented as mean ± SD and analyzed by ordinary one-way ANOVA followed by post-hoc Tukey's multiple comparisons test when ANOVA showed significant differences. No differences were seen in Psd95 [ANOVA summary, $F(2, 15) = 0.1105$, $p = 0.8961$ (ns)]. Significant difference was observed in mBri2 expression [ANOVA summary, $F(2, 15) = 26.33$, $p < 0.0001$ ****, post-hoc Tukey's multiple comparisons test: *Itm2b^{WT/WT}* versus *Itm2b^{B/B}*, $p < 0.0001$ ****, *Itm2b^{WT/WT}* versus *Itm2b^{D/D}*, $p < 0.0001$ ****, *Itm2b^{B/B}* versus *Itm2b^{D/D}*, $p > 0.05$ ns].

Itm2b and excitatory transmission



membranes. In contrast, chloroquine treatment caused exclusively a considerable accumulation of BRI2-ABri and BRI2-ADan in *Itm2b^{B/B}* and *Itm2b^{D/D}* neurons, respectively (Fig. 5, A–B).

Discussion

Our studies suggest that BRI2-ADan and BRI2-ABri may be targeted for ERLAD. The evidence that ADan and ABri peptides tend to aggregate and form amyloid deposits (2, 3) is consistent with the hypothesis that the immature mutant BRI2 proteins, which contain these sequences at the COOH-terminus, may misfold in the ER (Fig. 6). However, a fraction of BRI2-ADan and BRI2-ABri must escape lysosomal degradation and traffic through the *trans*-Golgi where a convertase removes the ADan and ABri peptides, since: 1) ADan and ABri peptides are produced in humans carrying the Danish and British mutation, respectively (2, 3); 2) cells transfected with *ITM2b^{F-D}* and *ITM2b^{F-B}*, *Itm2b^{B/B}* and *Itm2b^{D/D}* brain lysates and primary neurons contain some mBri2 (Figs. 2–5). In the central nervous system, these maturation anomalies lead to partial loss of mBri2 in synaptoneurosome (Fig. 2), reduced

glutamatergic neurotransmitter release, and AMPAR-mediated responses in *Itm2b^{B/B}* and *Itm2b^{D/D}* animals (Fig. 1).

Although future studies are needed to assess whether these excitatory synapses dysfunctions described here are pathologically relevant, the evidence presented here is noteworthy because also other genes mutated in Familial forms of dementia, such as *APP*, *PSEN1*, and *PSEN2*, are implicated in glutamatergic synaptic transmission. *APP* modulates glutamate release (12–15), a function that is altered by a pathogenic *APP* mutation (the Swedish mutation) (15). In addition, long-term potentiation (LTP), a cellular surrogate for memory and memory impairment caused by extracellular Aβ and Tau oligomers are *APP*-dependent (16). *PSEN1* and *PSEN2* regulate glutamate release by a presynaptic mechanism, a function that is altered by pathogenic mutation (17–19). Finally, a genetic variant of *TREM2* that increases risk of sporadic AD in humans changes glutamatergic transmission (20) in a rat KI model (21). Our findings that BRI2 also physiologically fine-tunes glutamate transmission with both pre- and postsynaptic mechanisms and that pathogenic mutations dysregulate this function are intriguing and support the hypothesis that defects in excitatory neurotransmitter release may

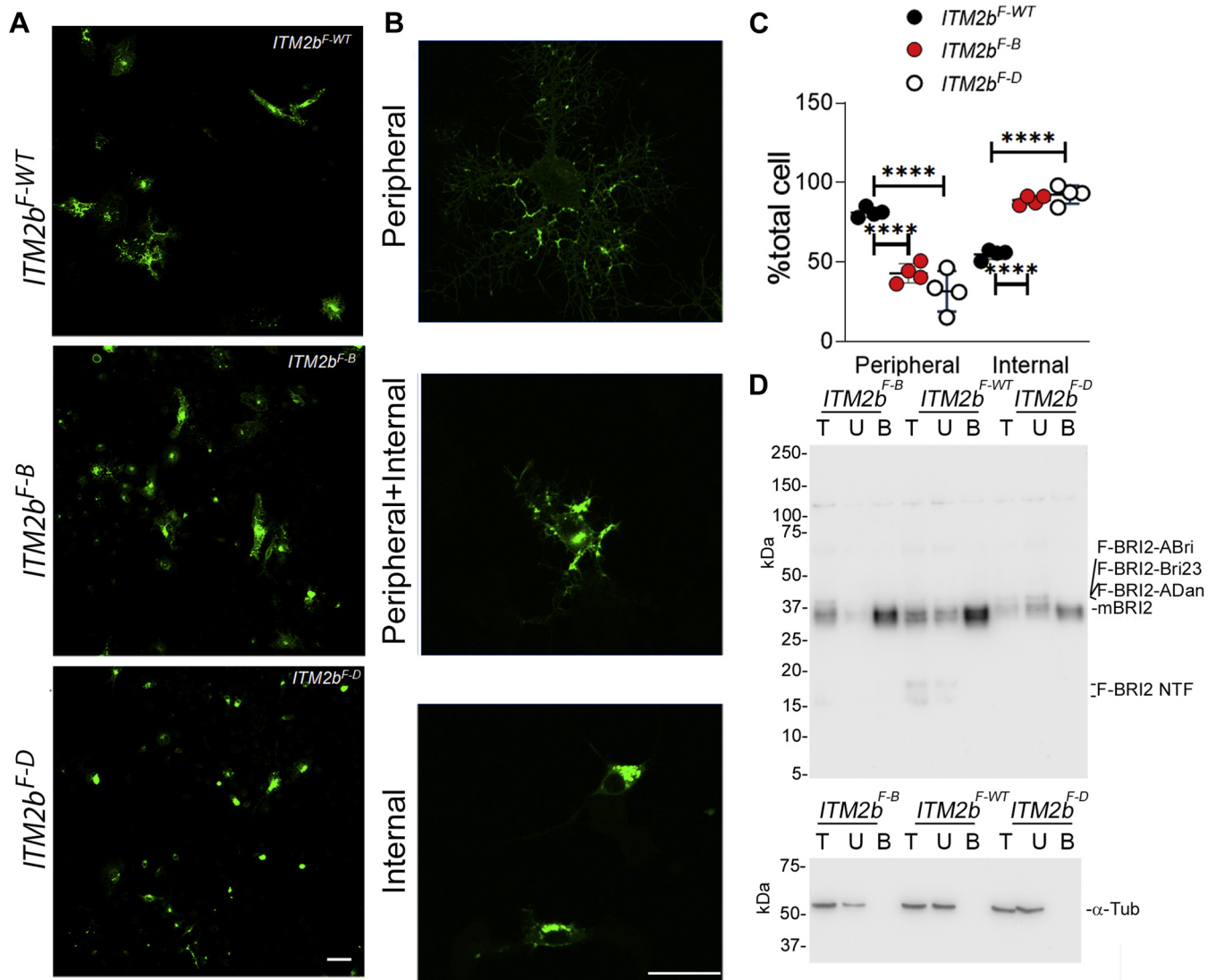


Figure 4. Distinct subcellular distribution of wild-type and mutant BRI2 forms in N2A transfected cells. N2A cells were transfected with *Flag-ITM2b^{F-WT}*, *Flag-ITM2b^{F-B}*, and *Flag-ITM2b^{F-D}* constructs for 24 h and differentiated by 2 μ M Retinoic acid for 24 h. **A**, immunocytochemistry staining with anti-Flag M2-FITC, scale bar = 50 μ m. **B**, samples of peripheral and internal BRI2 staining used for the quantitative analysis. **C**, quantitative analysis of cell numbers with different BRI2 distributions. Data are represented as mean \pm SD and analyzed by ordinary two-way ANOVA followed by post-hoc Tukey's multiple comparisons test when ANOVA showed significant differences [ANOVA summary, $F_{\text{interaction}(2,18)} = 99.55, p < 0.0001, F_{\text{BRI2 constructs}}(1,18) = 99.04, p < 0.0001, F_{\text{distribution type}}(2, 27) = 1.699, p = 0.2109$, post-hoc Tukey's multiple comparisons test: Peripheral: *ITM2b^{F-WT}* versus *ITM2b^{F-B}*, $p < 0.0001^{****}$, *ITM2b^{F-WT}* versus *ITM2b^{F-D}*, $p < 0.0001^{****}$, *ITM2b^{F-B}* versus *ITM2b^{F-D}*, $p > 0.05$ ns. Internal: *ITM2b^{F-WT}* versus *ITM2b^{F-B}*, $p < 0.0001^{****}$, *ITM2b^{F-WT}* versus *ITM2b^{F-D}*, $p < 0.0001^{****}$, *ITM2b^{F-B}* versus *ITM2b^{F-D}*, $p > 0.05$ ns]. **D**, biotinylation of transfected N2A cells shows that only mBRI2 traffics to the plasma membrane.

represent a general and convergent mechanism leading to neurodegeneration.

Years ago, we proposed that familial Danish, British, and Alzheimer's dementias may share a pathogenic sameness. This hypothesis was based on the following evidence: 1) APP and BRI2 physically interact (9, 22–24); 2) BRI2 alters APP processing (9, 24, 25); 3) APP and APP processing mediate LTP deficits as well as learning and memory deficits of Danish and British KI mice (26–31). In this context, the evidence that both APP and BRI2 tune excitatory synaptic transmission and that these functions are altered by pathogenic mutations in both APP and BRI2 is intriguing and suggests that APP and BRI2 may functionally interact if in tuning glutamatergic transmission. Future studies will be needed to test this hypothesis.

Experimental procedures

Mice and ethics statement

Mice were handled according to the Ethical Guidelines for Treatment of Laboratory Animals of the NIH. The procedures were described and approved by the Institutional Animal Care and Use Committee (IACUC, protocol number PROTO201702513).

Mice slice preparation

Mice were deeply anesthetized with isoflurane and intracardially perfused with an ice-cold cutting solution containing (in mM) 120 choline chloride, 2.6 KCl, 26 NaHCO₃, 1.25 NaH₂PO₄, 0.5 CaCl₂, 7 MgCl₂, 1.3 ascorbic acid, 15 glucose,

Itm2b and excitatory transmission

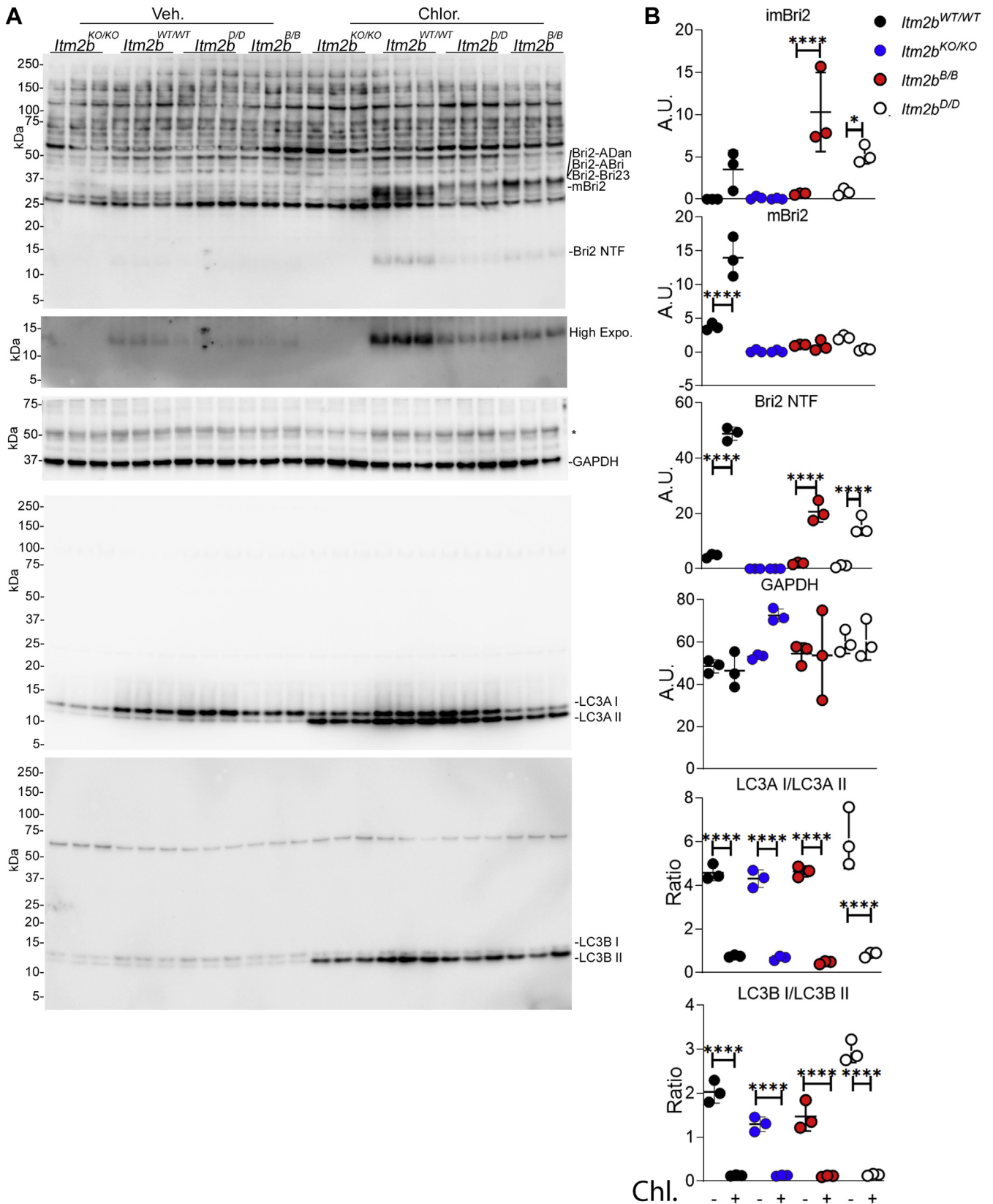


Figure 5. Distinct degradation pathways of wild-type and mutant Bri2 forms in primary neuron isolated from *Itm2b*^{WT/WT}, *Itm2b*^{B/B}, and *Itm2b*^{D/D} mice. *A*, western immunoblot analysis of primary hippocampal neurons isolated from *Itm2b*^{WT/WT}, *Itm2b*^{KO/KO}, *Itm2b*^{B/B}, and *Itm2b*^{D/D} P1 pups treated with 50 μ M chloroquine for 18 h. *B*, quantification of imBri2, mBri2, Bri2 NTF, GAPDH, and LC3A/B levels. Data are represented as mean \pm SD and analyzed by ordinary two-way ANOVA followed by post-hoc Sidak's multiple comparisons test when ANOVA showed significant differences [ANOVA summary, LC3A: $F_{\text{interaction}(3,16)} = 2.99$, $p = 0.0621$, $F_{\text{treatment}(1, 16)} = 395$, $p < 0.0001$, $F_{\text{genotype}(3, 16)} = 4.645$, $p = 0.0161$, post-hoc Sidak's multiple comparisons test: *Itm2b*^{WT/WT}: veh versus Chlor, $p < 0.0001$ ****, *Itm2b*^{KO/KO}: veh versus Chlor, $p < 0.0001$ ****, *Itm2b*^{B/B}: veh versus Chlor, $p < 0.0001$ ****, *Itm2b*^{D/D}: veh versus Chlor,

prebubbled with 95% O₂/5% CO₂ for 15 min. The brains were rapidly removed from the skull. Coronal brain slices containing the hippocampal formation (350 μm thick) were prepared in the ice-cold cutting solution bubbled with 95% O₂/5% CO₂ using Vibratome VT1200S (Leica Microsystems) and then incubated in an interface chamber in ACSF containing (in mM): 126 NaCl, 3 KCl, 1.2 NaH₂PO₄; 1.3 MgCl₂, 2.4 CaCl₂, 26 NaHCO₃, and 10 glucose (at pH 7.3), bubbled with 95% O₂ and 5% CO₂ at 30 °C for 1 h, and then kept at room temperature. The hemi-slices were transferred to a recording chamber perfused with ACSF at a flow rate of ~2 ml/min using a peristaltic pump. Experiments were performed at 28.0 °C ± 0.1 °C.

Whole-cell electrophysiological recording

Whole-cell recordings in the voltage-clamp mode (-70 mV) were made with patch pipettes containing (in mM): 132.5 Cs-gluconate, 17.5 CsCl, 2 MgCl₂, 0.5 EGTA, 10 HEPES, 4 ATP, and 5 QX-314, with pH adjusted to 7.3 by CsOH. Patch pipettes (resistance, 8–10 MΩ) were pulled from 1.5 mm thin-walled borosilicate glass (Sutter Instruments, Novato, CA) on a horizontal puller (model P-97; Sutter Instruments, Novato, CA). Basal synaptic responses were evoked at 0.05 Hz by electrical stimulation of the Schaffer collateral afferents using concentric bipolar electrodes. CA1 neurons were viewed under upright microscopy (FN-1, Nikon Instruments, Melville, NY) and recorded with Axopatch-700B amplifier (Molecular Devices, San Jose, CA). Data were low-pass filtered at 2 kHz and acquired at 5 to 10 kHz. The series resistance (Rs) was consistently monitored during recording in case of reseal of ruptured membrane. Cells with Rs >20 MΩ or with Rs deviated by >20% from initial values were excluded from analysis. Excitatory postsynaptic currents (EPSCs) were recorded in ACSF containing 15 μM bicuculline methiodide to block GABA-A receptors. The stimulation intensity was adjusted to evoke EPSCs that were 40% of the maximal evoked amplitudes (“test intensity”). 5 to 10 min after membrane rupture, EPSCs were recorded for 7 min at a test stimulation intensity that produced currents of ~40% maximum. For recording of paired-pulse ratio (PPR), paired-pulse stimuli with 50 ms or 200 ms interpulse interval were given. The PPR was calculated as the ratio of the second EPSC amplitude to the first. For recording of AMPA/NMDA ratio, the membrane potential was firstly held at -70 mV to record only AMPAR current for 20 sweeps with 20 s intervals. Then the membrane potential was turned to +40 mV to record NMDAR current for 20 sweeps with perfusion of

5 μM NBQX to block AMPAR. Mini EPSCs were recorded by maintaining neurons at -70 mV with ACSF containing 1 μM TTX and 15 μM bicuculline methiodide to block action potentials and GABA-A receptors, respectively. mEPSCs were recorded for 5 to 10 min for analysis. Data were collected and analyzed using the Axopatch 700B amplifiers and pCLAMP10 software (Molecular Devices), and mEPSCs are analyzed using mini Analysis Program.

Mice brain preparation and synaptoneurosomes preparation

Mouse brain fractionations were prepared as follows. Brains were homogenized (w/v = 100 mg tissue/1 ml buffer) in buffer A (5 mM HEPES, 1 Mm MgCl₂, 0.5 mM CaCl₂, PH7.4) supplemented with protease/phosphatase inhibitor (Thermo Fisher Scientific 78440) on ice. Homogenate was centrifuged at 1400g for 10 min. The supernatant was collected and labeled as S1 fraction. S1 was centrifuged at 13,800g for 10 min to generate pellet. The pellet was resuspended in 300ul buffer B (0.32 M sucrose, 6 mM Tris, pH 8.0), layered a discontinuous sucrose gradient (0.85, 1.0 and 1.2 M sucrose, 6 mM Tris, pH 8.0), and centrifuged at 83,000g for 2 h. SP fraction was present as a white band at the 1.0/1.2 M interface. The SP fraction was lysed with Buffer T (5% Triton X-100, 6 mM Tris, pH 8.0) to achieve final Triton-X 100 concentration to 0.5%. After 15 min shaking on ice, samples were centrifuged at 20,000g for 20 min. The separated supernatant was collected and labeled as Triton soluble (SPs) fraction. The pellet was resuspended in 50 ml Buffer T and was labeled as Triton insoluble (SPi) fraction.

scRNA-seq analysis

Full project data was downloaded from the Mouse Development Atlas (32). The full expression values and metadata were downloaded in loom format and imported to Seurat for additional analyses. Cells expression values were normalized using SCTransform and clustered following the standard workflow (33). Cluster markers were transferred from the development atlas to ensure parity with cell classifications. For cell coexpression of molecules, a normalized value of 1 was considered positive for the query gene of interest, and the expression of Itm2b was pulled for each positive cell for comparative visualization.

Plasmids

Constructs of Flag-human full-length BRI2 (*ITM2b^{F-WT}*) in pcDNA3.1 was previously described (24). Flag-FBD mutant BRI2 (*ITM2b^{F-B}*) and Flag-FDD mutant BRI2 (*ITM2b^{F-D}*) were

p < 0.0001****. LC3B: $F_{interaction(3,16)} = 24.53, p < 0.0001, F_{treatment(1,16)} = 599.7, p < 0.0001, F_{genotype(3,16)} = 25.99, p < 0.0001$, post-hoc Sidak’s multiple comparisons test:*Itm2b^{WT/WT}*: veh versus Chlor, *p* < 0.0001****, *Itm2b^{KO/KO}*: veh versus Chlor, *p* < 0.0001****, *Itm2b^{B/B}*: veh versus Chlor, *p* < 0.0001****, *Itm2b^{D/D}*: veh versus Chlor, *p* < 0.0001****. imBri2: $F_{interaction(3,16)} = 6.934, p = 0.0033, F_{treatment(1,16)} = 32.33, p < 0.0001, F_{genotype(3,16)} = 8.668, p = 0.0012$, post-hoc Sidak’s multiple comparisons test:*Itm2b^{WT/WT}*: veh versus Chlor, *p* = 0.1377 ns, *Itm2b^{KO/KO}*: veh versus Chlor, *p* > 0.9999 ns, *Itm2b^{B/B}*: veh versus Chlor, *p* < 0.0001****, *Itm2b^{D/D}*: veh versus Chlor, *p* = 0.0434*. mBri2: $F_{interaction(3,16)} = 37.01, p < 0.0001, F_{treatment(1,16)} = 21.15, p = 0.0003, F_{genotype(3,16)} = 80.73, p < 0.0001$, post-hoc Sidak’s multiple comparisons test:*Itm2b^{WT/WT}*: veh versus Chlor, *p* < 0.0001****, *Itm2b^{KO/KO}*: veh versus Chlor, *p* > 0.9999 ns, *Itm2b^{B/B}*: veh versus Chlor, *p* = 0.9998 ns, *Itm2b^{D/D}*: veh versus Chlor, *p* = 0.2465 ns. Bri2 NTF: $F_{interaction(3,16)} = 126.4, p < 0.0001, F_{treatment(1,16)} = 558.6, p < 0.0001, F_{genotype(3,16)} = 187.7, p < 0.0001$, post-hoc Sidak’s multiple comparisons test:*Itm2b^{WT/WT}*: veh versus Chlor, *p* < 0.0001****, *Itm2b^{KO/KO}*: veh versus Chlor, *p* > 0.9999 ns, *Itm2b^{B/B}*: veh versus Chlor, *p* < 0.0001****, *Itm2b^{D/D}*: veh versus Chlor, *p* < 0.0001****. GAPDH: $F_{interaction(3,16)} = 1.825, p = 0.1833, F_{treatment(1,16)} = 1.325, p = 0.2667, F_{genotype(3,16)} = 3.320, p = 0.0466$, post-hoc Sidak’s multiple comparisons test:*Itm2b^{WT/WT}*: veh versus Chlor, *p* = 0.9978 ns, *Itm2b^{KO/KO}*: veh versus Chlor, *p* = 0.0769 ns, *Itm2b^{B/B}*: veh versus Chlor, *p* > 0.9999 ns, *Itm2b^{D/D}*: veh versus Chlor, *p* > 0.9999 ns.].

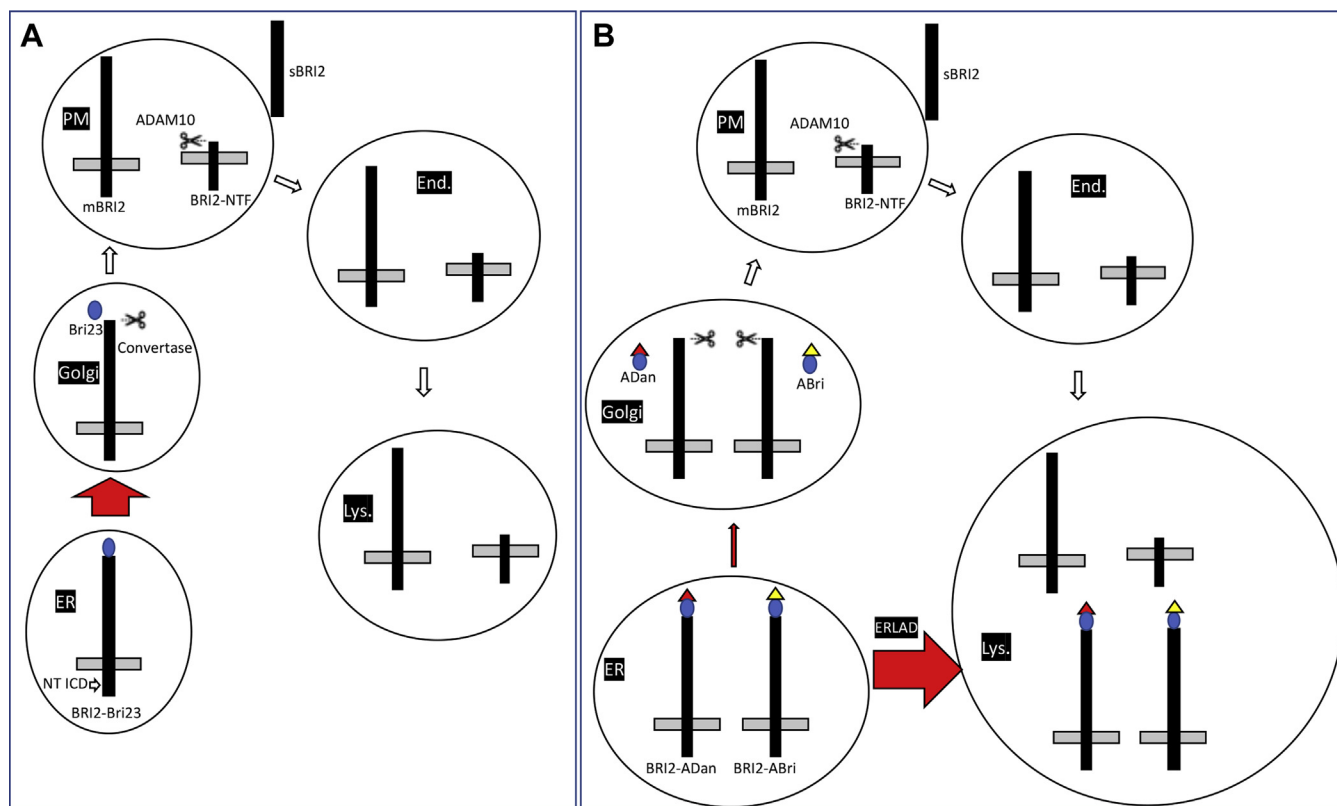


Figure 6. Modeling wild-type and mutant BRI2 maturation, trafficking, and degradation. A, BRI2 is synthesized in the ER as an immature precursors (BRI2-Bri23) that is cleaved in the Golgi apparatus at the C-terminus by proprotein convertase to produce the mature (mBRI2) and the COOH-terminal peptide Bri23. mBRI2 is transported to the plasma membrane where it can undergo an additional cleavage by ADAM10 in its ectodomain. This cleavage releases sBRI2 and the membrane-bound BRI2-NTF. Both mBRI2 and BRI2-NTF are endocytosed and degraded by the lysosomes. B, the Danish mutation changes the last amino acid of BRI2 and adds 11 additional amino acids at the COOH-terminus. The British mutations add 11 extra amino acids, which are different from those added by the Danish mutation, at the COOH-terminus as well. A fraction of immature mutant Danish (BRI2-ADan) and British (BRI2-ABri) BRI2 traffic to the Golgi where convertase cleavage generates mBRI2 and two distinct 34 amino acid long peptides, called ADan and ABri, respectively. ADan and ABri can form amyloid fibrils. It is important noting that mBRI2 produced by these pathogenic precursors is identical to the wild-type mBRI2. Large fractions of BRI2-ADan and BRI2-ABri are targeted for ERLAD. It is likely that the ADan and ABri sequences may cause misfolding of BRI2-ADan and BRI2-ABri in the ER.

both obtained by mutagenesis of *ITM2b*^{F-WT}. *ITM2b*^{F-B} expressed the extra C-terminal 11 amino acids long sequence “RTVKKNIIEEN”. In *ITM2b*^{F-D} the last amino acid, a Ser (S), is replaced by “FNLFLNSQEKHY.”

Cell culture and transfection

Neuro-2A (N2A) cells (ATCC CCL-131) and HeLa cells (ATCC CCL-2) were maintained in Eagle’s Minimum Essential Medium (EMEM) (Gibco 11095-098) supplemented with 10% fetal bovine serum and Antibiotic-Antimycotic (Gibco 15240112). Both HeLa cells and N2A cells were transfected with indicated plasmids *via* Fugene kit (Promega, E2311) as previously described (34–36).

Immunocytochemistry and cell counting

The N2A cells were plated on coverslips precoated with poly L-lysine (Sigma, P4707). Twenty-four hours after transfection, N2A cells were differentiated by 0.1% FBS and 2 mM retinoic acid for 24 h. Differentiated N2A cells were washed with PBS, fixed by 4% PFA, permeabilized with 0.1% Triton X-100 in PBS, blocked with 10% BSA in PBS, incubated with Anti-Flag M2 FITC (Sigma, F4049), and visualized on confocal

microscope (Nikon A1R). For cell counting, we replicated n = 4 independent transfection and took ten nonoverlapped images for each transfection. An average of 250 cells were counted for each transfection.

Biotinylation, streptavidin precipitation

Biotinylation experiments were performed as described (9). Twenty-four hours after transfection, HeLa cells or N2A cells were washed three times with cold PBS plus Ca²⁺ and Mg²⁺ (PBS-CM) and labeled for 30 min on ice in 0.5 mg/ml sulfo-NHS-SS-biotin (Pierce) dissolved in PBS-CM. Media was removed by washing three times with PBS-CM containing 0.1% BSA. The cells were lysed in RIPA buffer (10 mM Tris-Cl, 1 mM EDTA, 0.5 mM EGTA, 1% Triton X-100, 0.1% SDS, 140 mM NaCl). The lysates were cleared by centrifuging at 20,000g for 10 min and were mixed with streptavidin agarose beads (Sigma S1638). After collecting unbound lysate (U), the beads were washed four times with the RIPA buffer and were boiled in 2× SDS buffer (B). Comparable volume of the samples was subjected to Western immunoblot. The streptavidin precipitants correspond to five times of total lysates or unbound proteins.

Table 1
List of antibodies used

Antibody	Brand	Cat. #	Host	Type	Usage	note
α -tubulin	Sigma-Aldrich	T6199	Mouse	monoclonal	1:1000	
Bri2-N terminus	D'Adamo's lab		Rabbit	polyclonal	6 μ g/ml	Raised against peptide "AQKEAKKDEPKSSE"
NMDA R2B	Cell Signaling Technology	4212	Rabbit	monoclonal	1:1000	
PSD95	Cell Signaling Technology	2507	Rabbit	polyclonal	1:1000	
Vamp2	Synaptic Systems	104,211	Mouse	monoclonal	1:1000	
Flag-hrp	Sigma-Aldrich	A8592	Mouse	monoclonal	1:1000	
Flag- <i>fitc</i>	Sigma-Aldrich	F4049	Mouse	monoclonal	1:1000	
LC3A	Cell Signaling Technology	4599	Rabbit	monoclonal	1:1000	
LC3B	Cell Signaling Technology	2775	Rabbit	polyclonal	1:1000	
GAPDH	Sigma-Aldrich	G9545	Rabbit	polyclonal	1:1000	

Primary hippocampus neuron culture

Mouse hippocampus neurons were derived from *Itm2b*^{WT/WT}, *Itm2b*^{KO/KO}, *Itm2b*^{B/B}, and *Itm2b*^{D/D} postnatal day 0 mouse pups. Briefly, after the removal of adherent meninges, the hippocampi were collected in dissection media (HBSS w/o Mg and Ca, 1 mM sodium pyruvate, 0.1% glucose, 0.01 M HEPES). The hippocampi were dissected into single cell suspension with trituration following 15 min 37 °C 0.25% trypsin digestion. Cells were subsequently applied 0.1% Dnase (Sigma, dn25) and enriched in plating media (BME, 10% FBS, 0.09% Glucose, 1 mM Sodium Pyruvate, 2 mM Glutamine, 1 \times Pen/Strep). Cells were passed through Falcon 70 μ m nylon cell strainer and counted with Hemacytometer. 300k dissociated cells were plated in each single well in Poly L lysine pretreated 12-well-plate in 1 ml of maintenance media (Neurobasal media, 1 \times B-27, 2 mM glutamine, 1 \times Pen/Strep). Cells were refeed with 0.5 ml of maintenance media every 2 days. Cells were used for further treatment at DIV 14.

Pharmacological treatment and sample preparation

Primary neurons were treated with 50 mM Chloroquine (Cell signaling, 14774s) or same amount of PBS (Veh) for 18 h. Treated cell were washed with PBS and lysed in RIPA buffer with protease/phosphatase inhibitor for 15 min on ice. Lysed samples were centrifuged at full speed for 15 min. The supernatants were mix with LDS buffer supplemented with 10% β -mercapto-ethanol. Samples were boiled for 2 min before loading to a gel.

Western immunoblot analysis

Protein content quantified by Bradford analysis. Ten micrograms from each fraction was brought to 10 μ l with PBS and LDS buffer supplemented with 10% β -mercapto-ethanol and 8 M Urea. Denatured samples were loaded on a 4 to 12% Bis-Tris polyacrylamide gel (Bio-Rad, 3450125) and run at constant voltage (140 V). Proteins were transferred onto nitrocellulose membrane at 25 V for 7 min using *Trans*-blot Turbo system (Bio-Rad) and visualized by red Ponceau staining. Membranes were blocked with 5% nonfat dry milk (Bio-Rad, 1706404), washed with PBS/Tween-20 (0.05%), and applied primary antibody (see list and information about the dilution used in Table 1), which is diluted in blocking solution (Thermo Fisher Scientific, 37573) overnight at 4 °C.

Membranes were washed 3 \times 10 min and subsequently against by either HRP linked antimouse (SouthernBiotech, OB103105) or anti-rabbit (1:1 mix of SouthernBiotech, OB405005 and Cell Signaling Technology, 7074) at 1:1000 dilution for 45 min with shaking in room temperature. Membranes were developed with West Dura ECL reagent (Thermo Fisher Scientific, PI34076) and visualized on a ChemiDoc MP Imaging System (Bio-Rad). Signal intensity was quantified with Image Lab software (Bio-Rad). Data were analyzed using Prism software and represented as mean \pm SD.

Statistics

All the experiments mentioned in the paper were analyzed by one-way ANOVA or two-way ANOVA by indication. Data showing statistical significance by one-way ANOVA or two-way ANOVA were subsequently analyzed either by Tukey's multiple comparisons test or by Sidak's multiple comparisons. All statistical analyses were performed using Prism 8 (GraphPad) software.

Data availability

The data sets used and/or analyzed during the current study are available from the corresponding author on reasonable request.

Acknowledgments—All the authors read and approved the final manuscript.

Author contributions—L. D. generated the animals; T. Y. performed the biochemical and molecular experiments; W. Y. performed the electrophysiology experiments; A. D. analyzed the scRNA-Seq data; all the authors designed the experiments; L. D. and T. Y. wrote the paper.

Funding and additional information—L. D. was funded by the NIH/NIA R01AG052286, RF1AG064821-01, RF1AG064821-01, 1R01AG033007-01A109. The content is solely the responsibility of the authors and does not necessarily represent the official views of the National Institutes of Health.

Conflicts of interest—The authors declare that they have no conflicts of interest with the contents of this article.

Abbreviations—The abbreviations used are: EMEM, Eagle's Minimum Essential Medium; ERLAD, ER-to-lysosomes-associated degradation; FBD, familial British dementia; FDD, familial Danish

dementia; ISI, interstimulus interval; KI, knock-in; LTP, long-term potentiation; mEPSC, miniature excitatory postsynaptic currents; PPF, paired-pulse facilitation; PPR, paired-pulse ratio.

References

- Choi, S. I., Vidal, R., Frangione, B., and Levy, E. (2004) Axonal transport of British and Danish amyloid peptides via secretory vesicles. *FASEB J.* **18**, 373–375
- Vidal, R., Revesz, T., Rostagno, A., Kim, E., Holton, J. L., Bek, T., Bojsen-Møller, M., Braendgaard, H., Plant, G., Ghiso, J., and Frangione, B. (2000) A decamer duplication in the 3' region of the BRI gene originates an amyloid peptide that is associated with dementia in a Danish kindred. *Proc. Natl. Acad. Sci. U. S. A.* **97**, 4920–4925
- Vidal, R., Frangione, B., Rostagno, A., Mead, S., Révész, T., Plant, G., and Ghiso, J. (1999) A stop-codon mutation in the BRI gene associated with familial British dementia. *Nature* **399**, 776–781
- Yao, W., Yin, T., Tambini, M. D., and D'Adamio, L. (2019) The Familial dementia gene ITM2b/BRI2 facilitates glutamate transmission via both presynaptic and postsynaptic mechanisms. *Sci. Rep.* **9**, 4862
- Tamayev, R., Matsuda, S., Fa, M., Arancio, O., and D'Adamio, L. (2010) Danish dementia mice suggest that loss of function and not the amyloid cascade causes synaptic plasticity and memory deficits. *Proc. Natl. Acad. Sci. U. S. A.* **107**, 20822–20827
- Tamayev, R., Giliberto, L., Li, W., d'Abramo, C., Arancio, O., Vidal, R., and D'Adamio, L. (2010) Memory deficits due to familial British dementia BRI2 mutation are caused by loss of BRI2 function rather than amyloidosis. *J. Neurosci.* **30**, 14915–14924
- Giliberto, L., Matsuda, S., Vidal, R., and D'Adamio, L. (2009) Generation and initial characterization of FDD knock in mice. *PLoS One* **4**, e7900
- Zucker, R. S., and Regehr, W. G. (2002) Short-term synaptic plasticity. *Annu. Rev. Physiol.* **64**, 355–405
- Matsuda, S., Matsuda, Y., Snapp, E. L., and D'Adamio, L. (2011) Maturation of BRI2 generates a specific inhibitor that reduces APP processing at the plasma membrane and in endocytic vesicles. *Neurobiol. Aging* **32**, 1400–1408
- Martin, L., Fluhrer, R., Reiss, K., Kremmer, E., Saftig, P., and Haass, C. (2008) Regulated intramembrane proteolysis of Bri2 (Itm2b) by ADAM10 and SPPL2a/SPPL2b. *J. Biol. Chem.* **283**, 1644–1652
- Fregno, I., and Molinari, M. (2019) Proteasomal and lysosomal clearance of faulty secretory proteins: ER-associated degradation (ERAD) and ER-to-lysosome-associated degradation (ERLAD) pathways. *Crit. Rev. Biochem. Mol. Biol.* **54**, 153–163
- Fanutza, T., Del Prete, D., Ford, M. J., Castillo, P. E., and D'Adamio, L. (2015) APP and APLP2 interact with the synaptic release machinery and facilitate transmitter release at hippocampal synapses. *Elife* **4**, e09743
- Fogel, H., Frere, S., Segev, O., Bharill, S., Shapira, I., Gazit, N., O'Malley, T., Slomowitz, E., Berdichevsky, Y., Walsh, D. M., Isacoff, E. Y., Hirsch, J. A., and Slutsky, I. (2014) APP homodimers transduce an amyloid-beta-mediated increase in release probability at excitatory synapses. *Cell Rep.* **7**, 1560–1576
- Yao, W., Tambini, M. D., Liu, X., and D'Adamio, L. (2019) Tuning of glutamate, but not GABA, release by an intra-synaptic vesicles APP domain whose function can be modulated by beta- or alpha-secretase cleavage. *J. Neurosci.* **39**, 6992–7005
- Tambini, M. D., Yao, W., and D'Adamio, L. (2019) Facilitation of glutamate, but not GABA, release in familial Alzheimer's APP mutant knock-in rats with increased beta-cleavage of APP. *Aging Cell* **18**, e13033
- Puzzo, D., Piacentini, R., Fá, M., Gulisano, W., Li Puma, D. D., Staniszewski, A., Zhang, H., Tropea, M. R., Cocco, S., Palmeri, A., Fraser, P., D'Adamio, L., Grassi, C., and Arancio, O. (2017) LTP and memory impairment caused by extracellular A β and Tau oligomers is APP-dependent. *Elife* **6**, e26991
- Wu, B., Yamaguchi, H., Lai, F. A., and Shen, J. (2013) Presenilins regulate calcium homeostasis and presynaptic function via ryanodine receptors in hippocampal neurons. *Proc. Natl. Acad. Sci. U. S. A.* **110**, 15091–15096
- Zhang, D., Zhang, C., Ho, A., Kirkwood, A., Sudhof, T. C., and Shen, J. (2010) Inactivation of presenilins causes pre-synaptic impairment prior to post-synaptic dysfunction. *J. Neurochem.* **115**, 1215–1221
- Xia, D., Watanabe, H., Wu, B., Lee, S. H., Li, Y., Tsvetkov, E., Bolshakov, V. Y., Shen, J., and Kelleher, R. J., 3rd (2015) Presenilin-1 knockin mice reveal loss-of-function mechanism for familial Alzheimer's disease. *Neuron* **85**, 967–981
- Ren, S., Yao, W., Tambini, M. D., Yin, T., Norris, K. A., and D'Adamio, L. (2020) Microglia. *Elife* **9**, e57513
- Tambini, M. D., and D'Adamio, L. (2020) Trem2 splicing and expression are preserved in a human abeta-producing, rat knock-in model of trem2-R47H Alzheimer's risk variant. *Sci. Rep.* **10**, 4122
- Matsuda, S., Giliberto, L., Matsuda, Y., Davies, P., McGowan, E., Pickford, F., Ghiso, J., Frangione, B., and D'Adamio, L. (2005) The familial dementia BRI2 gene binds the Alzheimer gene amyloid-beta precursor protein and inhibits amyloid-beta production. *J. Biol. Chem.* **280**, 28912–28916
- Fotinoupolou, A., Tsachaki, M., Vlavaki, M., Pouloupoulos, A., Rostagno, A., Frangione, B., Ghiso, J., and Efthimiopoulos, S. (2005) BRI2 interacts with amyloid precursor protein (APP) and regulates amyloid beta (A β) production. *J. Biol. Chem.* **280**, 30768–30772
- Matsuda, S., Giliberto, L., Matsuda, Y., McGowan, E. M., and D'Adamio, L. (2008) BRI2 inhibits amyloid beta-peptide precursor protein processing by interfering with the docking of secretases to the substrate. *J. Neurosci.* **28**, 8668–8676
- Matsuda, S., Tamayev, R., and D'Adamio, L. (2011) Increased A β PP processing in familial Danish dementia patients. *J. Alzheimers Dis.* **27**, 385–391
- Tamayev, R., Matsuda, S., Giliberto, L., Arancio, O., and D'Adamio, L. (2011) APP heterozygosity averts memory deficit in knockin mice expressing the Danish dementia BRI2 mutant. *EMBO J.* **30**, 2501–2509
- Tamayev, R., and D'Adamio, L. (2012) Inhibition of γ -secretase worsens memory deficits in a genetically congruous mouse model of Danish dementia. *Mol. Neurodegener.* **7**, 19
- Tamayev, R., and D'Adamio, L. (2012) Memory deficits of British dementia knock-in mice are prevented by A β -precursor protein haploinsufficiency. *J. Neurosci.* **32**, 5481–5485
- Tamayev, R., Matsuda, S., Arancio, O., and D'Adamio, L. (2012) β - but not γ -secretase proteolysis of APP causes synaptic and memory deficits in a mouse model of dementia. *EMBO Mol. Med.* **4**, 171–179
- Lombino, F., Biundo, F., Tamayev, R., Arancio, O., and D'Adamio, L. (2013) An intracellular threonine of amyloid- β precursor protein mediates synaptic plasticity deficits and memory loss. *PLoS One* **8**, e57120
- Biundo, F., Ishiwari, K., Del Prete, D., and D'Adamio, L. (2016) Deletion of the γ -secretase subunits Aph1B/C impairs memory and worsens the deficits of knock-in mice modeling the Alzheimer-like familial Danish dementia. *Oncotarget* **7**, 11923–11944
- Zeisel, A., Hochgerner, H., Lönnerberg, P., Johnson, A., Memic, F., van der Zwan, J., Häring, M., Braun, E., Borm, L. E., La Manno, G., Codeluppi, S., Furlan, A., Lee, K., Skene, N., Harris, K. D., et al. (2018) Molecular architecture of the mouse nervous system. *Cell* **174**, 999–1014. e1022
- Hafemeister, C., and Satija, R. (2019) Normalization and variance stabilization of single-cell RNA-seq data using regularized negative binomial regression. *Genome Biol.* **20**, 296
- Scheinfeld, M. H., Roncarati, R., Vito, P., Lopez, P. A., Abdallah, M., and D'Adamio, L. (2002) Jun NH2-terminal kinase (JNK) interacting protein 1 (JIP1) binds the cytoplasmic domain of the Alzheimer's beta-amyloid precursor protein (APP). *J. Biol. Chem.* **277**, 3767–3775
- Scheinfeld, M. H., Matsuda, S., and D'Adamio, L. (2003) JNK-interacting protein-1 promotes transcription of A beta protein precursor but not A beta precursor-like proteins, mechanistically different than Fe65. *Proc. Natl. Acad. Sci. U. S. A.* **100**, 1729–1734
- Scheinfeld, M. H., Ghersi, E., Davies, P., and D'Adamio, L. (2003) Amyloid beta protein precursor is phosphorylated by JNK-1 independent of, yet facilitated by, JNK-interacting protein (JIP)-1. *J. Biol. Chem.* **278**, 42058–42063